land

MDPI

Article

Spatiotemporal Evolution and Correlation Analysis of Carbon Emissions in the Nine Provinces along the Yellow River since the 21st Century Using Nighttime Light Data

Yaohui Liu [1,2], Wenyi Liu [1], Peiyuan Qiu [1,*], Jie Zhou [3,4] and Linke Pang [1]

[1] School of Surveying and Geo-Informatics, Shandong Jianzhu University, Jinan 250101, China
[2] College of Geodesy and Geomatics, Shandong University of Science and Technology, Qingdao 266590, China
[3] Institute of Geology, China Earthquake Administration, Beijing 100029, China
[4] Key Laboratory of Seismic and Volcanic Hazards, China Earthquake Administration, Beijing 100029, China
* Correspondence: qiupeiyuan20@sdjzu.edu.cn

Abstract: Monitoring carbon emissions is crucial for assessing and addressing economic development and climate change, particularly in regions like the nine provinces along the Yellow River in China, which experiences significant urbanization and development. However, to the best of our knowledge, existing studies mainly focus on national and provincial scales, with fewer studies on municipal and county scales. To address this issue, we established a carbon emission assessment model based on the "NPP-VIIRS-like" nighttime light data, aiming to analyze the spatiotemporal variation of carbon emissions in three different levels of nine provinces along the Yellow River since the 21st century. Further, the spatial correlation of carbon emissions at the county level was explored using the Moran's *I* spatial analysis method. Results show that, from 2000 to 2021, carbon emissions in this region continued to rise, but the growth rate declined, showing an overall convergence trend. Per capita carbon emission intensity showed an overall upward trend, while carbon emission intensity per unit of GDP showed an overall downward trend. Its spatial distribution generally showed high carbon emissions in the eastern region and low carbon emissions in the western region. The carbon emissions of each city mainly showed a trend of "several"; that is, the urban area around the Yellow River has higher carbon emissions. Meanwhile, there is a trend of higher carbon emissions in provincial capitals. Moran's *I* showed a trend of decreasing first and then increasing and gradually tended to a stable state in the later stage, and the pattern of spatial agglomeration was relatively fixed. "High–High" and "Low–Low" were the main types of local spatial autocorrelation, and the number of counties with "High–High" agglomeration increased significantly, while the number of counties with "Low–Low" agglomeration gradually decreased. The findings of this study provide valuable insights into the carbon emission trends of the study area, as well as the references that help to achieve carbon peaking and carbon neutrality goals proposed by China.

Keywords: carbon emissions; nighttime lights; spatiotemporal variation; spatial correlation; nine provinces along the Yellow River

Citation: Liu, Y.; Liu, W.; Qiu, P.; Zhou, J.; Pang, L. Spatiotemporal Evolution and Correlation Analysis of Carbon Emissions in the Nine Provinces along the Yellow River since the 21st Century Using Nighttime Light Data. *Land* **2023**, *12*, 1469. https://doi.org/10.3390/land12071469

Academic Editors: Chao Wang, Jinyan Zhan and Xueting Zeng

Received: 27 June 2023
Revised: 17 July 2023
Accepted: 21 July 2023
Published: 23 July 2023

1. Introduction

Since the Industrial Revolution, increasing carbon emissions from human activities have become a major contributor to global climate change. As a result, climate change has become a pressing global issue, garnering attention from the international community [1–3]. To develop and implement climate change mitigation and adaptation policies and plans, there is an urgent need for accurate, reliable, and real-time carbon emission data [4,5]. Consequently, monitoring and evaluating carbon emissions has become a critical priority and research hotspot, which helps ecological environment protection and prompts high-quality development.

In recent years, a growing amount of research has been conducted on studying the spatiotemporal characteristics, and monitoring and evaluation of carbon emissions [6–9]. Researchers have investigated various factors that influence carbon emissions in different regions and proposed predictive models to forecast carbon emissions in specific areas. For instance, Huang et al. [10] analyzed the carbon peak and carbon emission information of the Yangtze River Economic Belt, and proposed a support vector regression (SVR) machine prediction model to predict the carbon emission information in the region. Du et al. [11] established a China Carbon Watch (CCW) system, enabling the monthly calculation of carbon emissions from provincial-level urban and rural households between January and May 2020. Liu et al. [12] used the Lasso regression model to screen out eight significant factors affecting carbon emissions based on the data of Jiangsu province from 2001 to 2018 and used the BP neural network model to predict the carbon emissions of Jiangsu province from 2019 to 2030. Ning et al. [13] established a prediction model for carbon emissions in four representative provinces and cities in Beijing, Henan, Guangdong, and Zhejiang from 1997 to 2017. However, the abovementioned research lacks the capability of achieving small-scale refined monitoring, such as at the county level, and cannot provide real-time monitoring and assessment of carbon emissions. Therefore, new methods and technologies are highly needed to enable more granular, comprehensive, and real-time monitoring and assessment of carbon emissions.

Nighttime light remote sensing is an optical remote sensing technology that detects and obtains information on nighttime lights, providing a quick, accurate, and objective view of the surface and human activities [14–16]. Unlike daytime remote sensing, nighttime light remote sensing can reveal information that is not visible during the day [17,18]. Since most of the stable light at night comes from artificial sources in urban areas, remote sensing images of nighttime lights can more intuitively reflect differences in human activity at night [19–22]. Nighttime light data has become a new monitoring method with the advantages of large coverage, fast timeliness, and convenient access, making it suitable for multi-scale and long-term research on urban issues [23]. Nighttime light data has been used in many studies related to disaster monitoring, urban sprawl, and human activity [24–28]. For instance, Fan et al. [29] used NPP-VIIRS nighttime light data to monitor recovery after earthquakes and quickly assess earthquake damage. Li et al. [30] researched the variation of nighttime illumination in different seismic regions and the influence of human activities on nighttime illumination. Liu et al. [31] used NPP-VIIRS nighttime light data to explore the resilience and post-disaster recovery of Zhengzhou City, using the extremely heavy rainstorm in Zhengzhou City on July 20, 2021 as an example. Chen et al. [32] constructed a new nighttime light landscape indicator, taking various townships in Fujian Province as examples to reveal rural and urban economic development, and their differences and economic expansion from multiple perspectives.

Nighttime light data has also been used to explore carbon emissions [33–37]. Doll et al. [38] produced the world's first 1 × 1 resolution carbon emission distribution map, revealing the difference in carbon emission levels of countries at different stages of development based on the correlation between DMSP-OLS nighttime light data and carbon emissions. Sun et al. [39] monitored the variation in China's city-level carbon emissions from 2000 to 2017 based on nighttime light data, and found that low-carbon cities are concentrated in western and central China, while high-carbon-emission cities are mainly distributed in the Beijing–Tianjin–Hebei and Yangtze River Delta regions. Yang et al. [40] established a regional Chinese building carbon emission calculation model based on the nighttime light data and building carbon emission data in the eastern, central, and western regions of China. Guo et al. [41] analyzed the spatiotemporal variation patterns, correlations, and heterogeneity of carbon emissions of three different administrative units from 2012 to 2019 based on nighttime light data and normalized difference vegetation index. Overall, nighttime light remote sensing is an effective tool for monitoring human activity and carbon emissions, providing valuable information for urban and environmental studies,

and has the potential to contribute significantly to the development of urban planning and environmental management policies.

Located in the central and western regions of China, the nine provinces along the Yellow River are important areas for achieving coordinated regional development. This region is China's main energy and heavy chemical industry base, containing high-carbon industries such as coal, oil, steel, and chemicals, resulting in the issues of carbon emissions of this region being more prominent [42–44]. The development of this region can promote the economic development of the western region, narrow the development gap between the eastern and western regions, and achieve a balanced and coordinated national economy. In addition, the development of this region also has a significant impact on the development of the global economy, which can promote the vitality of global trade and investment. To achieve the coordinated development of economic development and environmental protection, the Chinese government has adopted a series of policies and measures to promote the construction of ecological civilization and energy conservation, and emission reduction, and strive to achieve the goals of carbon peak and carbon neutrality. However, to the best of our knowledge, existing studies mainly focus on the national and provincial scales and fewer studies are conducted at the municipal and county scales. This inevitably ignores the development stage and regional differences, which is not conducive to the national level and all levels of government developing practical carbon reduction and pollution reduction programs based on local conditions while improving the quality of economic development and steadily promoting the urbanization process. Therefore, the monitoring and analysis of carbon emissions at the municipal and county levels in the region will help the government adjust its policies on time, optimize the industrial and energy structures, accelerate green and low-carbon development, promote economic transformation and upgrading, and achieve sustainable economic development.

This study aims to investigate the spatiotemporal variation, per capita carbon emission intensity, and carbon emission intensity per unit of GDP in the nine provinces along the Yellow River since the 21st century. We first build a fitting model for carbon emission monitoring and evaluation using "NPP-VIIRS-like" nighttime light data and other multi-source data. The spatiotemporal evolution characteristics of carbon emissions at municipal and county levels are monitored and assessed. Furthermore, Moran's I is employed to investigate the spatial correlations of carbon emissions at county levels in the region. This study provides important reference information for decision-making departments to formulate more reasonable and effective carbon emission reduction policies to optimize the industrial structure of this region and reduce carbon emissions.

This study has the following three main objectives:

1. Construct a fitting model of the nighttime lighting index and carbon emissions for the timely and accurate prediction of carbon emissions;
2. Investigate the spatiotemporal characteristics and trends of carbon emissions in the nine provinces along the Yellow River of China since the 21st century;
3. Explore the spatial correlation of carbon emissions at the county level using Moran's I statistical method.

The rest of this study is organized as follows: Section 2 describes the study area and data. Section 3 introduces the calculation method of carbon emissions, the processing method of nighttime lighting data, the fitting model construction, and the spatial correlation analysis method. Section 4 introduces the spatiotemporal variation of carbon emissions and the fitting model of the nine provinces along the Yellow River. The discussion and conclusion are presented in Sections 5 and 6, respectively.

2. Study Area and Data

2.1. Study Area

The Yellow River is considered the "mother river" of China. This massive river, one of the longest in the world and the second longest in China, is located in the northern part of the country. The Yellow River basin encompasses a vast area that includes nine

provinces: Shanxi, Inner Mongolia, Shandong, Henan, Sichuan, Shaanxi, Gansu, Qinghai, and Ningxia, as depicted in Figure 1. This region covers a staggering 3,569,000 km^2, which constitutes around 37.2% of China's entire territory. As of 2022, the population of this region is approximately 420 million people, accounting for 29.8% of China's total population. Additionally, the GDP of this region is estimated at 28.7 trillion yuan, which is equivalent to 25.1% of China's overall GDP. The Yellow River basin is a crucial area for China's economy and culture, with a rich history and a vibrant present. Moreover, this region is rich in biodiversity and ecosystems, including wetlands, forests, grasslands, and rivers. These ecosystems are vital to maintaining the ecological balance of the region, protecting rare species, and preserving natural ecological functions. Protecting the ecosystems along the nine Yellow Provinces will help maintain the stability of the global ecosystem.

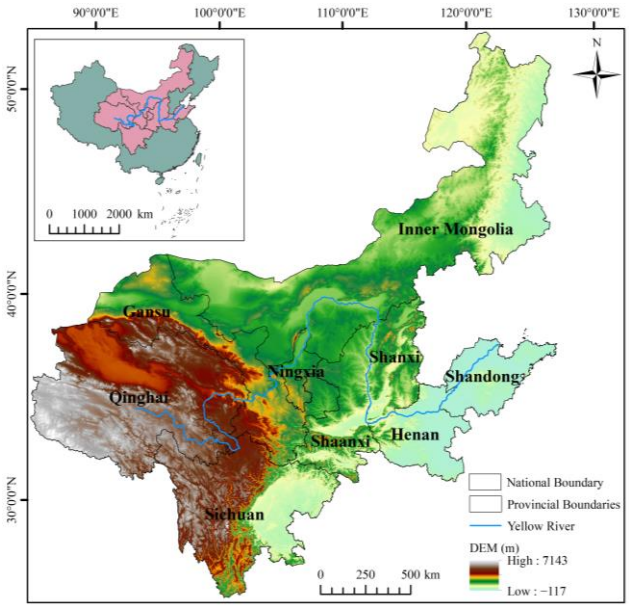

Figure 1. Geographical location of the study area.

2.2. Data

To conduct a comprehensive analysis of carbon emissions in the study area, various energy data, including raw coal, coke, crude oil, gasoline, kerosene, diesel, fuel oil, natural gas, heat, and electricity, were selected. The energy statistics were obtained from the Statistical Yearbook, China Energy Statistical Yearbook, and Urban Greenhouse Gas Inventory Research of nine provinces and cities from 2000 to 2021. To estimate carbon emissions in the study area, "NPP-VIIRS-like" nighttime light data from 2000 to 2021 were obtained from the AI-Earth Earth Science Cloud Platform (https://engine-aiearth.aliyun.com, accessed on 15 March 2023). The spatial resolution of this data is 500 m, which has the advantages of high spatial resolution, global coverage, long-term continuous observation, and strong data consistency and comparability, and provides a powerful tool for researchers to analyze and understand the distribution and changes of nighttime lights on the Earth's surface, and can be used to construct a reliable model for monitoring and evaluating carbon emissions [45–47]. Population and GDP data were also collected from the Statistical Yearbooks of nine provinces and cities from 2000 to 2021. Table 1 shows the data-related information, including data name, time range, and sources of data.

Table 1. Data sources in this study.

Data	Time Range	Data Sources
Energy statistics	2000–2021	Statistical Yearbook, China Energy Statistical Yearbook, Urban Greenhouse Gas Inventory Research of nine provinces and cities
"NPP-VIIRS-like" nighttime light data	2000–2021	AI-Earth Earth Science Cloud Platform (https://engine-aiearth.aliyun.com)
Population and GDP data	2000–2021	Statistical Yearbooks of nine provinces and cities

3. Methodology

In this study, we focused on assessing the spatiotemporal variation of the carbon emissions in the nine provinces along the Yellow River since the 21st century based on nighttime light remote sensing and multisource data. The overall workflow of this study is presented in Figure 2.

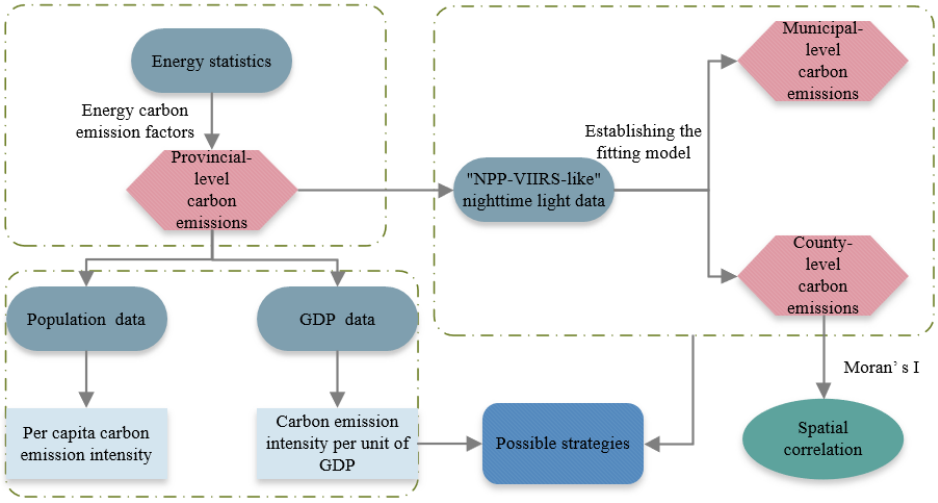

Figure 2. The workflow of this study.

3.1. Calculation of Carbon Emissions

To estimate the carbon emissions of each province in the study area, this study uses the 2006 Greenhouse Gas Emissions Inventory published by the IPCC (Intergovernmental Panel on Climate Change) [48]. The carbon emissions are calculated using the following equation:

$$CO_2 = \frac{44}{12} \times \sum_{i=1}^{10} K_i E_i \quad (1)$$

where i is 10 energy types; E_i is the consumption of energy i in terms of standard coal (10,000 tons); and K_i is the carbon emission factor of energy i (10,000 carbon)/(10,000 standard coal), from the default value of IPCC carbon emission calculation guidelines, where the original data unit is J. To be consistent with the statistical data unit, it is converted into standard coal with a conversion factor of 1×10^4 tons of standard coal equal to 2.93×10^5 GJ. The carbon emission factors for each type of energy are presented in Table 2 [49].

Table 2. Energy carbon emission factors.

Energy Type	Raw Coal	Coke	Crude Oil	Gasoline	Kerosene	Diesel	Fuel Oil	Natural Gas	Heat	Electricity
Converted to standard coal (tons of standard coal/ton)	0.7143	0.9714	1.4286	1.4714	1.4714	1.4751	1.4286	1.33	34.12	0.345
Carbon emission factor (10^4 tons carbon/10^4 tons standard coal)	0.7559	0.855	0.5857	0.5538	0.5714	0.5921	0.6185	0.4483	0.67	0.272

3.2. Per Capita Carbon Emission Intensity and Carbon Emission Intensity Per Unit of GDP

To obtain a comprehensive understanding of carbon emission patterns and mechanisms, this study integrates the demographic and economic statistics of each province. The aim is to investigate the spatiotemporal distribution characteristics and influence factors of per capita carbon emission intensity and carbon emission intensity per unit of GDP in each province, with the following equations:

$$\text{Per capita carbon emission intensity} = CO_2 / p \tag{2}$$

$$\text{Carbon emission intensity per unit of GDP} = CO_2 / GDP \tag{3}$$

where CO_2 is total carbon emissions (10,000 tons); p is the year-end resident population data (10,000 people); and GDP is gross regional product (10,000 yuan).

3.3. Nighttime Light Index Calculation

For this study, the total nighttime light index ($TNLI$) is selected as the index for calculation and analysis. $TNLI$ is calculated as the sum of the light digital number (DN) values of administrative units, as presented by the following equation:

$$TNLI = \sum_{i=1}^{n} DN_i \tag{4}$$

where n is the number of rasters and DN_i is the radiation value of the image element corresponding to each raster.

3.4. Establishing the Fitting Model

Given the significant correlation between $TNLI$ and carbon emissions, we used a linear regression model to fit the $TNLI$ and total carbon emissions of the study area. In this model, the intercept was set to 0, reflecting the absence of energy-related carbon emissions in unlit regions. The equation for the linear regression model is as follows:

$$CO_2 = a \times TNLI \tag{5}$$

where CO_2 is the total carbon emission, $TNLI$ is the total nighttime light index, and a is the fitting factor.

From 2000 to 2021, the TNLI and carbon emissions of nine provinces showed an approximate linear growth in the early years, and then reached the inflection point and gradually slowed down. Moreover, carbon emissions were affected by the phased emission reduction targets and tasks proposed by China's government in 2009 and 2015, and the growth rate had shown a rapid downward trend. Therefore, considering the inherent attributes of the data in conjunction with the temporal milestones associated with carbon emission mitigation policies, it has been delineated into seven distinct temporal intervals to conduct a comprehensive fitting analysis. The outcomes of this analysis are presented in Table 3, where a denotes the fitting coefficient of carbon emissions and TNLI, and R^2 denotes the correlation coefficient of carbon emissions and TNLI: the larger this value, the stronger the correlation.

Table 3. Parameters of the quadratic polynomial model of carbon emissions from 2000 to 2021.

Year	*a*	R^2
2000–2004	0.1465	0.9208
2005–2008	0.1763	0.9483
2009–2012	0.2079	0.9602
2013–2014	0.1410	0.9016
2015–2016	0.1439	0.9007
2017–2018	0.1059	0.8485
2019–2021	0.0858	0.7813

3.5. Spatial Correlation

To investigate the spatiotemporal dynamics of carbon emissions, we employ global Moran's *I* and local indicators of spatial association (LISA). Global Moran's *I* is calculated using Equation (6), with values ranging from −1 to 1. Values closer to 1 indicate a stronger positive correlation, while values closer to −1 indicate a stronger negative correlation. Values close to 0 indicate a lack of significant correlation. Local Moran's *I* is calculated using Equation (7). LISA analysis is used to describe the correlation of spatial units based on five attributes: "High–High", "Low–Low", "High–Low", "Low–High", and "Not Significant".

$$I = \frac{\sum_{i=1}^{n}\sum_{j=1}^{n}\omega_{ij}(x_i-\overline{x})(x_j-\overline{x})}{\frac{1}{n}\sum_{i=1}^{n}(x_i-\overline{x})^2\cdot\sum_{i=1}^{n}\sum_{j=1}^{n}\omega_{ij}} \quad (6)$$

$$I_i = \frac{x_i-\overline{x}}{\frac{1}{n}\sum_{i=1}^{n}(x_i-\overline{x})^2}\sum_{j=1,j\neq i}^{n}\omega_{ij}(x_j-\overline{x}) \quad (7)$$

where n is the number of regions, x_i is the carbon emissions of the ith region, the upper horizontal line represents the mean value, and ω_{ij} is the spatial symmetric weight.

4. Results

4.1. Temporal Characteristics of Provincial-Level Carbon Emissions

The carbon emissions of the study area from 2000 to 2021 are presented in Figure 3. Since the 21st century, the total carbon emissions of this region have continued to rise, but the growth rate has gradually decreased, showing an overall trend of convergence. It is worth noting that, despite this convergence, the region has not yet reached peak carbon. In 2000, the total carbon emissions were 890.849 million tons; in 2012, they reached 3440.83 million tons; and, in 2021, they increased to 3787.586 million tons. The total carbon emissions continued to rise, but the average annual growth rate showed a downward trend: the average annual growth rate of carbon emissions from 2000 to 2012 was 12.01%, and it fell rapidly to 1.10% from 2012 to 2021. This demonstrates that the emission reduction targets and tasks established by China at the Copenhagen Conference in 2009 and the 75th session of the United Nations General Assembly in 2020 [50] have an important impact on carbon emission reduction in the Yellow River Basin. Figure 4 shows the share of carbon emissions upstream of the Yellow River (including Qinghai, Inner Mongolia, Sichuan, Gansu, and Ningxia), the midstream (including Shaanxi and Shanxi), and the downstream (including Henan and Shandong). From 2000 to 2021, the difference between upstream and downstream carbon emission levels was small, accounting for about 80% of the carbon emissions of the nine Yellow River provinces, while the midstream carbon emissions accounted for a relatively small amount, about 20%. The proportion of upstream and midstream carbon emissions has gradually increased, from 31.41% in 2001 to 41.07% in 2021, and from 20.96% in 2005 to 22.14% in 2021. The upstream and midstream have been in pursuit of rapid economic development, and the resulting energy consumption has led to an increase in carbon emissions. The proportion of downstream carbon emissions showed a trend of first rising and then decreasing, rising from 43.88% in 2001 to 48.75% in 2005 and 36.79% in 2021. This is closely related to the shift of the focus of its economic development

from the early pursuit of rapid economic development to improving the high-quality and efficiency of economic development and optimizing the economic structure.

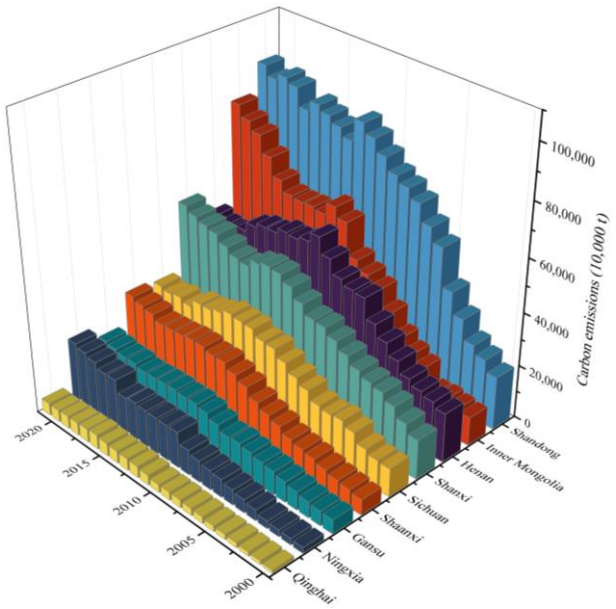

Figure 3. Temporal characteristics of provincial-level carbon emissions in the study area from 2000 to 2021.

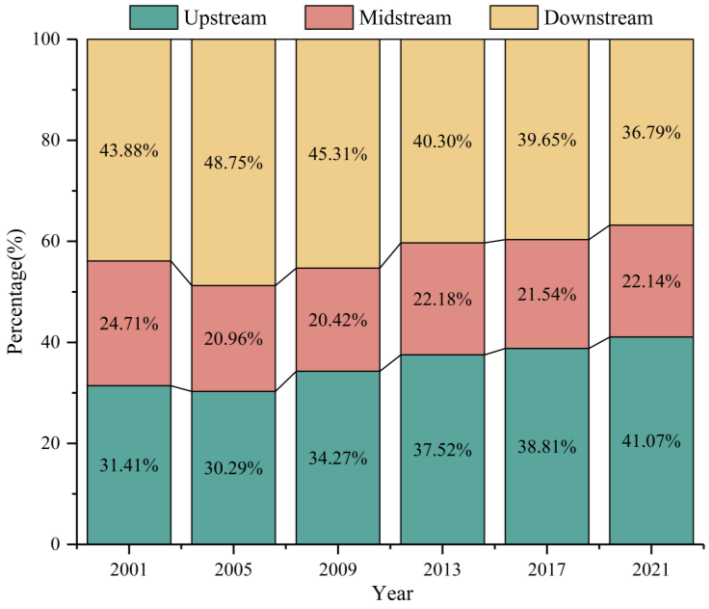

Figure 4. Percentage of carbon emissions in the study area from 2000 to 2021.

4.2. Spatial Characteristics of Provincial-Level Carbon Emissions

The spatial trends of carbon emissions of the study area from 2000 to 2021 are displayed in Figure 5. To investigate the spatial variation of carbon emissions across different regions and years, we employed the natural interruption point method to categorize the carbon emission data. Overall, carbon emissions from the nine Yellow River provinces show a trend of high in the east and low in the west. Specifically, the total carbon emissions of nine provinces along the Yellow River in 2001 were relatively low. In 2005, carbon emissions from Shandong, Shanxi, Henan, Inner Mongolia, Sichuan, and Gansu increased significantly, with Shandong's emissions exceeding 50 million tons. In 2013, carbon emissions in all four eastern provinces were at high levels. Shanxi's carbon emissions fell in 2017. This reduction

can be attributed to the successful implementation of an innovative initiative in Taiyuan, the provincial capital, wherein all taxis were electrified in 2016. However, carbon emissions in Shanxi and Shaanxi gradually increased in 2021, while those in Henan declined. This divergence can be attributed to the implementation of the "Notice on the Implementation of the Three-Year Action Plan for Energy Conservation and Carbon Reduction Transformation of Key Energy-using Units" by Henan province in 2021. The notice pointed out that, by 2023, key energy-using units will achieve an energy-saving capacity of more than 6 million tons of standard coal/year, and achieve maximum improvement in energy efficiency.

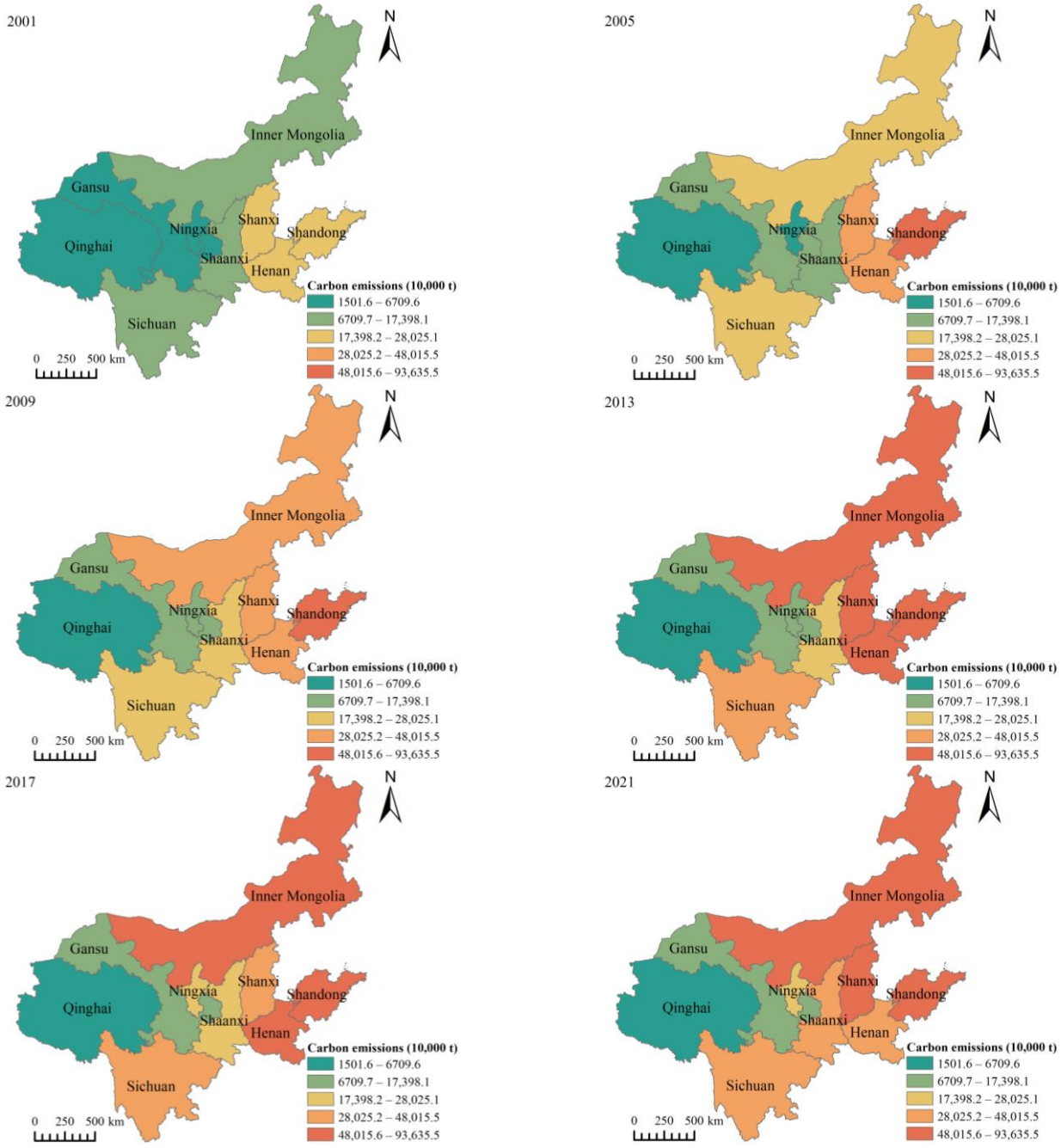

Figure 5. Spatial characteristics of provincial-level carbon emissions in the study area from 2000 to 2021.

4.3. Temporal Characteristics of Per Capita Carbon Emission Intensity and Carbon Emission Intensity Per Unit of GDP

The per capita carbon emission intensity is a crucial indicator of carbon emission levels and is the central critical issue in climate negotiations. It is important for developing effective carbon reduction strategies and for ensuring a sustainable future. The temporal characteristics of per capita carbon emission intensity in the study area from 2000 to 2021 are presented in Figure 6. From 2000 to 2021, the per capita carbon emission intensity of nine provinces along the Yellow River showed an overall upward trend. Among them, Inner Mongolia has the highest per capita carbon emission intensity, reaching 34.7 tons in 2021. Its growth trend is the largest, with an average annual growth rate of 10.94%. This is mainly due to its development mode of "relying on energy and relying on heavy energy", the characteristics of heavy industrial structure and high carbonization of energy structure, large stock and a high proportion of energy and raw material industries, and high energy consumption and high emission industries; renewable energy has become the main basic energy still to be developed, and the role of carbon emission reduction is not sufficient. Moreover, Ningxia's per capita carbon emission intensity is just below Inner Mongolia's, with a faster growth rate. Shanxi's per capita carbon emission intensity is in the middle of the range until it exceeds 15 tons in 2021. In contrast, Sichuan has the lowest per capita carbon emission intensity, at 3.4 tons. Its growth trend is also the smallest, with an average annual growth rate of 5.04%. This may be related to Sichuan's relatively clean industrial structure and relatively diversified energy structure, while Sichuan's vigorous development of renewable energy, such as hydropower and wind power, has also played a positive role in reducing carbon emissions. The per capita carbon emission intensity of the other provinces varies little, and they are all relatively low, located below 10 tons.

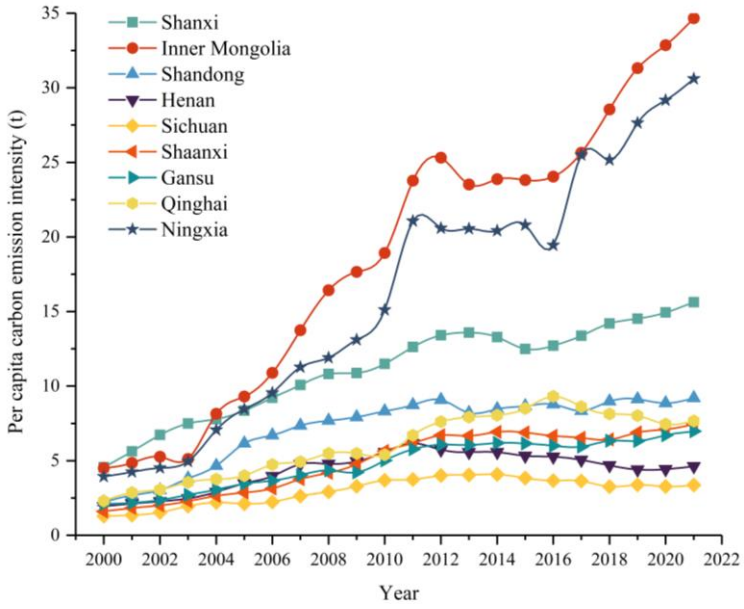

Figure 6. Temporal characteristics of per capita carbon emission intensity in the study area from 2000 to 2021.

The carbon emission intensity per unit of GDP is an internationally recognized indicator for measuring the effectiveness of emission reduction. The temporal characteristics of the carbon emission intensity per unit of GDP in the study area from 2000 to 2021 are presented in Figure 7. From 2000 to 2021, the carbon emission intensity per unit of GDP in the study area showed an overall downward trend. Ningxia has the highest carbon emission intensity per unit of GDP, reaching 4.9 tons/10,000 yuan in 2021. This is mainly because the energy structure of Ningxia is mainly based on coal, which accounts for a relatively high proportion of energy consumption. Moreover, Ningxia is a relatively underdeveloped

economic region, and, to catch up with the development speed of other regions, it may have neglected the importance of environmental protection in the process of economic development. There may be some lag in the utilization of resources and transformation of industrial structure, resulting in a high carbon emission intensity per unit GDP. Sichuan, on the other hand, has the smallest carbon emission intensity per unit of GDP, as low as 0.5 tons/10,000 yuan in 2021. This is due to Sichuan's active development of other new energy sources, and the utilization of these clean energy sources has helped to reduce its dependence on traditional high-carbon energy sources, further reducing the carbon emission intensity per unit of GDP. Moreover, Sichuan's economic structure is relatively lightweight. Lightweight industries usually have a relatively low energy demand, thus reducing the carbon emission intensity per unit of GDP. Henan has been actively restructuring and transforming its energy mix over the past few years. Consequently, Henan has the largest downward trend in carbon emission intensity per unit of GDP, with an average annual reduction rate of 6.97%. By contrast, due to Ningxia's relatively homogenous energy structure, the energy transition and emission reduction efforts face greater challenges. Consequently, Ningxia has the smallest downward trend in carbon emission intensity per unit of GDP, with an average annual reduction rate of 1.48%.

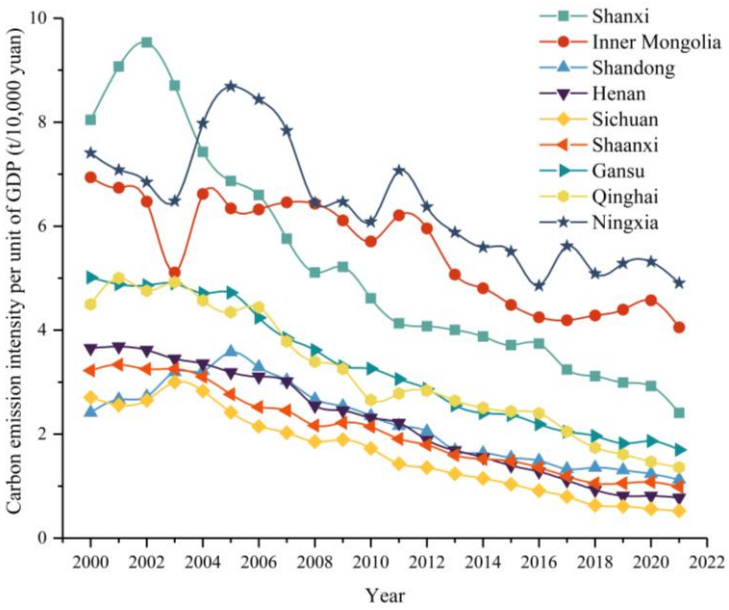

Figure 7. Temporal characteristics of carbon emission intensity per unit GDP in the study area from 2000 to 2021.

4.4. Spatial Characteristics of Municipal-Level Carbon Emissions

Based on the fitting model proposed above and the nighttime light index at the municipal scale, the inversion obtained the spatial characteristics of municipal-level carbon emissions in the study area from 2000 to 2021 (as presented in Figure 8). From 2000 to 2021, the carbon emissions of this region mainly showed a trend of "several"; that is, the carbon emissions of urban areas around the Yellow River were higher, and the carbon emissions of provincial capitals were higher. From 2000 to 2009, carbon emissions increased rapidly, and the proportion of cities with high carbon emissions increased from 4.35% in 2001 to 32.17% in 2021. In 2001, only Jinan, Qingdao, Yantai, Zhengzhou, and Taiyuan had high levels of carbon emissions. In 2021, only the eastern and northern cities had faster carbon emission growth, while the southwestern cities had a slower growth rate. Shandong is a province with a large population and rapid economic development, accounting for about 9% of the country's carbon emissions in 2020, making it the largest carbon emitter province in China. Moreover, Shandong is also the largest coal power province in China, accounting for 9.5% of the country's installed capacity. More than 99% of its heat demand is met by coal, with

the rest coming from oil and gas. Therefore, in 2021, only Rizhao in Shandong had carbon emissions of less than 30 million tons.

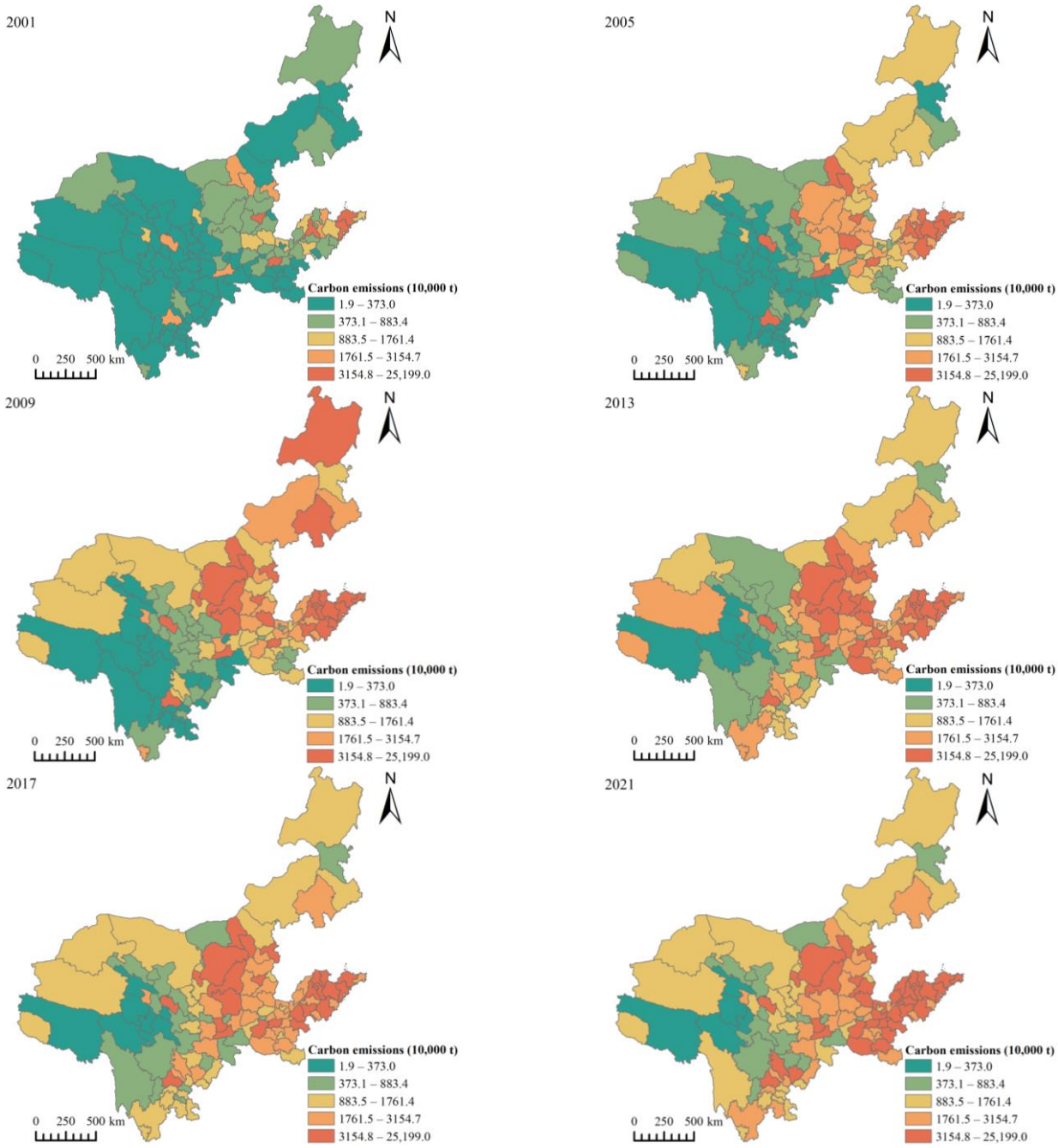

Figure 8. Spatial characteristics of municipal-level carbon emissions in the study area from 2000 to 2021.

4.5. Spatial Characteristics of County-Level Carbon Emissions

The spatial characteristics of county-level carbon emissions in the study area from 2000 to 2021 are presented in Figure 9. From 2000 to 2021, the carbon emissions of all districts and counties along this region increased significantly, showing a spatial distribution pattern of "southeast high and northwest low". Among them, counties in Shandong and Henan have higher carbon emissions, accounting for 91.97% and 81.65% of the high-carbon-emission counties in the two provinces in 2021. The growth rate of carbon emissions in each county and district showed a trend of "first urgent and then slow", with 2009 as the cut-off point.

The proportion of counties with high carbon emissions increased from 12.72% in 2001 to 40.56% in 2009 and 55.68% in 2021.

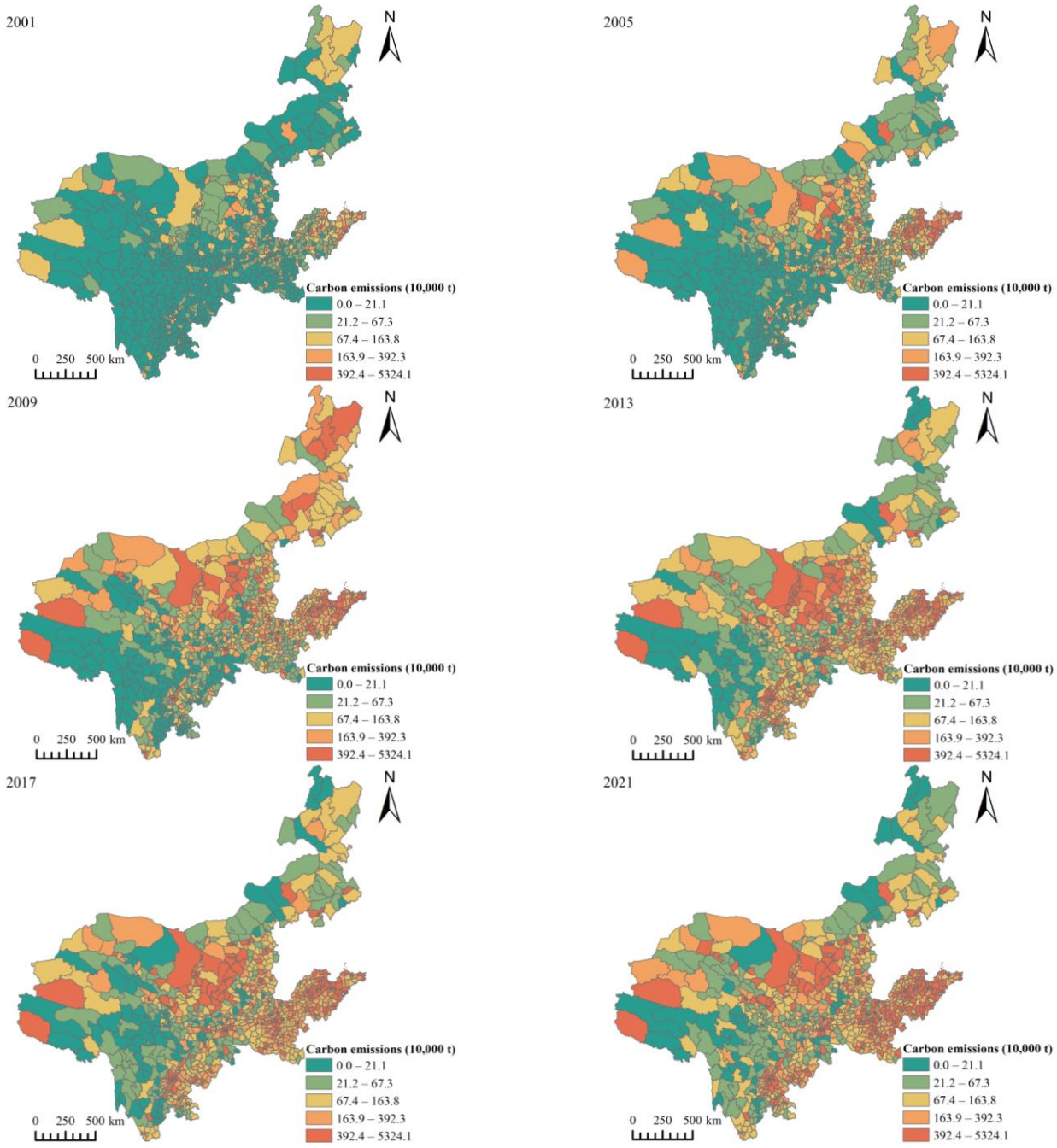

Figure 9. Spatial characteristics of county-level carbon emissions in the study area from 2000 to 2021.

5. Discussion

5.1. Global Spatial Correlation

GeoDa software was utilized to establish the spatial weights, and the global spatial correlation index (Moran's *I*) of county-level carbon emissions in the study area from 2000 to 2021 was calculated. The results are presented in Table 4. All the Moran's *I* of this region is positive, and the *p*-values are all zero, indicating a significant spatial correlation of county-level carbon emissions in the region. Moran's *I* shows a trend of decreasing first and then increasing and gradually tends to a stable state in the later stage, and the pattern of spatial agglomeration is relatively fixed. Before 2013, there was an overall downward

trend, from 0.314 in 2001 to 0.223 in 2013, indicating that counties with similar carbon emissions are more likely to be dispersed. This is because, since the beginning of the 21st century, all regions have made great efforts to build and develop, but the development has been uneven, resulting in different carbon emission levels. After 2013, the overall trend increased, from 0.223 in 2013 to 0.287 in 2021, and eventually stabilized, indicating that counties with similar carbon emissions are more inclined to agglomerate.

Table 4. Moran's *I* of county-level carbon emissions in the study area from 2000 to 2021.

Year	Moran's *I*	*p*
2001	0.314	0
2005	0.351	0
2009	0.313	0
2013	0.223	0
2017	0.270	0
2021	0.287	0

5.2. Local Spatial Correlation

The LISA clustering maps of county-level carbon emissions in the study area are presented in Figure 10. In general, the spatial agglomeration mode of county-level carbon emissions was relatively fixed, "High–High" and "Low–Low" were the main types of local spatial autocorrelation, and the number of counties and districts where "High–High" agglomeration increased significantly, while the number of counties and districts where "Low–Low" agglomeration gradually decreased. From 2000 to 2013, the "High–High" and "Low–High" types of counties and districts were mainly distributed along the Yellow River, and the number of "Low–High" types of districts and counties gradually increased, mainly because the counties along the Yellow River developed rapidly, but, due to uneven development caused by regional differences, most of the counties and districts along the coast had a "radiation effect" on surrounding cities, and carbon emissions formed the "High–High" type. Meanwhile, some counties and districts have a "siphon effect" on surrounding cities, and carbon emissions with a "Low–High" type. The "Low–Low" type is mainly distributed in Sichuan, which is because Sichuan's clean energy accounts for more than 80% to 90%, which is much higher than the national level, and the carbon emissions of each county are low. From 2013 to 2021, Shanxi's "High–High" and "Low–Low" gradually disappeared. The Sichuan Basin gradually formed the "High–High" type centered on Chengdu, and the number gradually increased. The "Low–Low" type in eastern Inner Mongolia and Yan'an and Linfen in Shaanxi is gradually increasing.

5.3. Possible Strategies

To prompt the ecological protection and high-quality development of the Yellow River Basin, the following strategies may be implemented:

(1) The upstream of the Yellow River should develop clean energy. The upstream of the Yellow River is rich in hydropower and wind energy resources, and vigorously develops hydropower and wind power to reduce the use of fossil energy and carbon emissions.

(2) The midstream of the Yellow River should promote industrial transformation and upgrading. The midstream of the Yellow River has a high degree of industrialization and should promote industrial transformation and upgrading, promote clean production technologies and circular economy models, reduce the use of fossil fuels, and reduce carbon emissions.

(3) The downstream of the Yellow River should promote green development. The downstream of the Yellow River comprises China's economic centers and urban agglomerations and should promote green development, encourage low-carbon consumption and lifestyles, and promote renewable energy and clean transportation.

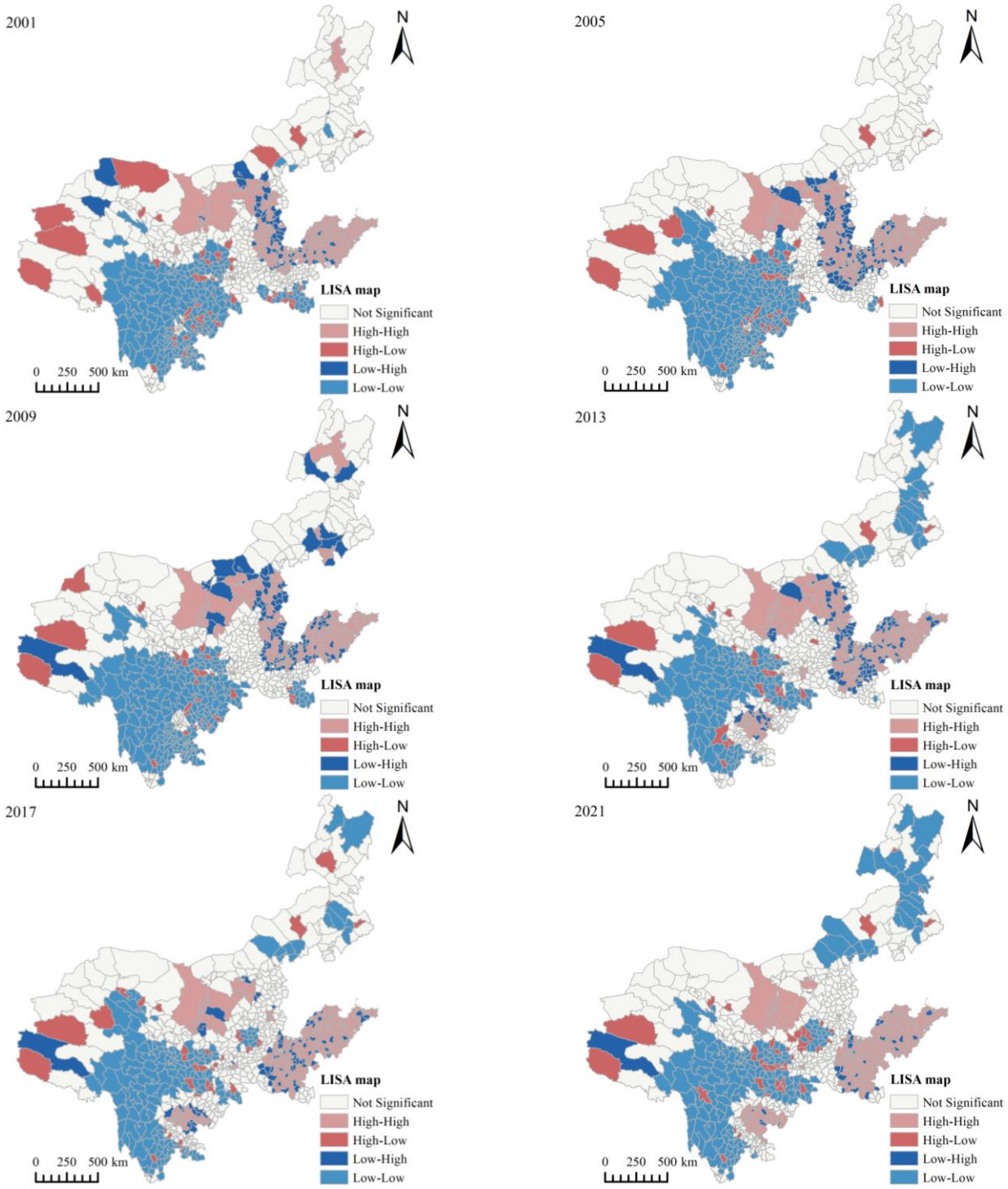

Figure 10. LISA map of county-level carbon emissions in the study area from 2000 to 2021.

6. Conclusions

This study establishes a carbon emission assessment model based on the "NPP-VIIRS-like" nighttime light data, investigating the spatiotemporal characteristics and trends of carbon emissions, per capita carbon emission intensity, and carbon emission intensity per unit of GDP in the study area since the 21st century. Further, the spatial correlation of carbon emissions at the county level is explored using the Moran's *I* spatial analysis method. This comprehensive method overcomes the limitations of incomplete traditional

statistics and differing statistical calibers, providing a reliable new tool for monitoring carbon emissions. The main conclusions drawn from this study are as follows:

(1) TNLI and carbon emission models of the study area were constructed according to different years. The model exhibited high accuracy with an average correlation coefficient R2 of 0.8945. The model has proven effective in estimating carbon emissions at the city and county levels, enabling the timely monitoring and assessment of carbon emissions in small-scale areas.

(2) In terms of temporal variation, from 2000 to 2021, carbon emissions in the study area continued to rise but the growth rate declined, showing an overall convergence trend, but not yet reaching a carbon peak. The proportion of upstream and midstream carbon emissions has gradually increased, while the proportion of downstream carbon emissions has gradually decreased. Per capita carbon emission intensity is generally on the rise, with Inner Mongolia having the largest per capita carbon intensity and Sichuan having the smallest. The carbon emission intensity per unit of GDP is generally declining. Ningxia has the highest carbon intensity per unit of GDP, while Sichuan has the lowest carbon intensity per unit of GDP.

(3) In terms of spatial variation, the carbon emissions of the study area generally show high carbon emissions in the eastern region and low carbon emissions in the western region. The carbon emissions of each city mainly show a trend of "several"; that is, the urban area around the Yellow River has higher carbon emissions. Meanwhile, there is a trend of higher carbon emissions in provincial capitals. The proportion of cities with high carbon emissions increased from 4.35% in 2001 to 32.17% in 2021. Counties in Shandong and Henan have higher carbon emissions, accounting for 91.97% and 81.65% of the two provinces in 2021, respectively.

(4) In terms of spatial relationship, Moran's *I* shows a trend of first decreasing and then increasing and gradually tends to a stable state in the later stage, and the pattern of spatial agglomeration is relatively fixed. "High–High" and "Low–Low" are the main types of local spatial autocorrelation, and the number of counties with "High–High" agglomeration increases significantly, while the number of counties with "Low–Low" agglomeration gradually decreases. From 2000 to 2013, counties of the "High–High" and "Low–High" types were mainly distributed along the Yellow River, and the "Low–Low" type was mainly distributed in Sichuan. From 2013 to 2021, Shanxi's "High–High" and "Low–Low" gradually disappeared. The Sichuan Basin gradually formed the "High–High" type centered on Chengdu, and the number gradually increased.

The spatial and temporal variations in carbon emissions show a converging trend of decreasing growth rates. While emissions continue to rise, the declining rate of growth suggests potential improvements in emission management and control measures. The rise in the per capita carbon emission intensity indicates the need for more sustainable and efficient use of resources. The decline in carbon emission intensity per unit of GDP indicates progress in decoupling economic growth from carbon emissions. Spatial differences in carbon emissions can be attributed to changes in economic activity, population density, and energy sources. Understanding these spatial differences can help target emission reduction strategies where they are most needed. Understanding the spatial relationships and patterns of carbon emissions can help policymakers to identify areas where targeted interventions are needed and to work together towards effective mitigation strategies. Taken together, these findings can guide policymakers in developing strategies and policies to mitigate carbon emissions, promote sustainable development, and achieve emission reduction targets.

This study presents a unique perspective on carbon emissions monitoring, providing valuable data references and decision-making support for governmental entities and businesses aiming to advance sustainable economic development and foster the establishment of ecological civilization. In our future research endeavors, we intend to delve deeper into the analysis of influencing factors and mechanisms associated with carbon

emissions, while also exploring effective monitoring technologies for carbon emissions based on heterogeneous data from multiple sources.

Author Contributions: Conceptualization, Y.L. and W.L.; methodology, W.L.; software, W.L.; validation, P.Q. and L.P.; formal analysis, Y.L.; investigation, J.Z.; resources, Y.L.; data curation, W.L.; writing—original draft preparation, W.L.; writing—review and editing, Y.L.; visualization, P.Q., J.Z. and L.P.; supervision, P.Q.; project administration, Y.L. and J.Z.; funding acquisition, Y.L. and P.Q. All authors have read and agreed to the published version of the manuscript.

Funding: This research was supported in part by the Natural Science Foundation of China, grant numbers 42001341, 42201077, and 42177453; the Natural Science Foundation of Shandong Province, grant number ZR2021QD074; and the China Postdoctoral Science Foundation, grant number 2023M732105.

Data Availability Statement: Data will be made available upon request.

Conflicts of Interest: The authors declare no conflict of interest.

References

1. Liu, Z.; Deng, Z.; Davis, S.J.; Giron, C.; Ciais, P. Monitoring global carbon emissions in 2021. *Nat. Rev. Earth Environ.* **2022**, *3*, 217–219. [CrossRef]
2. Wang, Y.; Guo, C.-H.; Du, C.; Chen, X.-J.; Jia, L.-Q.; Guo, X.-N.; Chen, R.-S.; Zhang, M.-S.; Chen, Z.-Y.; Wang, H.-D. Carbon peak and carbon neutrality in China: Goals, implementation path, and prospects. *China Geol.* **2021**, *4*, 720–746. [CrossRef]
3. Rising, J.A.; Taylor, C.; Ives, M.C.; Ward, R.E. Challenges and innovations in the economic evaluation of the risks of climate change. *Ecol. Econ.* **2022**, *197*, 107437. [CrossRef]
4. Khan, M.K.; Trinh, H.H.; Khan, I.U.; Ullah, S. Sustainable economic activities, climate change, and carbon risk: An international evidence. *Environ. Dev. Sustain.* **2022**, *24*, 9642–9664. [CrossRef]
5. Chen, L.; Msigwa, G.; Yang, M.; Osman, A.I.; Fawzy, S.; Rooney, D.W.; Yap, P.-S. Strategies to achieve a carbon neutral society: A review. *Environ. Chem. Lett.* **2022**, *20*, 2277–2310. [CrossRef] [PubMed]
6. Chuai, X.; Feng, J. High resolution carbon emissions simulation and spatial heterogeneity analysis based on big data in Nanjing City, China. *Sci. Total Environ.* **2019**, *686*, 828–837. [CrossRef]
7. Han, P.; Cai, Q.; Oda, T.; Zeng, N.; Shan, Y.; Lin, X.; Liu, D. Assessing the recent impact of COVID-19 on carbon emissions from China using domestic economic data. *Sci. Total Environ.* **2021**, *750*, 141688. [CrossRef]
8. Sun, S.; Xie, Y.; Li, Y.; Yuan, K.; Hu, L. Analysis of Dynamic Evolution and Spatial-Temporal Heterogeneity of Carbon Emissions at County Level along "The Belt and Road"—A Case Study of Northwest China. *Int. J. Environ. Res. Public Health* **2022**, *19*, 13405. [CrossRef]
9. Li, H.; Mu, H.; Zhang, M.; Gui, S. Analysis of regional difference on impact factors of China's energy–Related CO_2 emissions. *Energy* **2012**, *39*, 319–326. [CrossRef]
10. Huang, H.; Wu, X.; Cheng, X. The Prediction of Carbon Emission Information in Yangtze River Economic Zone by Deep Learning. *Land* **2021**, *10*, 1380. [CrossRef]
11. Du, M.; Zhang, X.; Xia, L.; Cao, L.; Zhang, Z.; Zhang, L.; Zheng, H.; Cai, B. The China Carbon Watch (CCW) system: A rapid accounting of household carbon emissions in China at the provincial level. *Renew. Sustain. Energy Rev.* **2022**, *155*, 111825. [CrossRef]
12. Liu, X.; Meng, X.; Wang, X. Carbon Emissions Prediction of Jiangsu Province Based on Lasso-BP Neural Network Combined Model. *IOP Conf. Ser. Earth Environ. Sci.* **2021**, *769*, 022017. [CrossRef]
13. Ning, L.; Pei, L.; Li, F. Forecast of China's Carbon Emissions Based on ARIMA Method. *Discret. Dyn. Nat. Soc.* **2021**, *2021*, 1441942. [CrossRef]
14. Liu, Y.; Liu, W.; Zhang, X.; Lin, Y.; Zheng, G.; Zhao, Z.; Cheng, H.; Gross, L.; Li, X.; Wei, B.; et al. Nighttime light perspective in urban resilience assessment and spatiotemporal impact of COVID-19 from January to June 2022 in mainland China. *Urban Clim.* **2023**, *50*, 101591. [CrossRef]
15. Shen, Y.; Chen, X.; Yao, Q.; Ding, J.; Lai, Y.; Rao, Y. Examining the Impact of China's Poverty Alleviation on Nighttime Lighting in 831 State-Level Impoverished Counties. *Land* **2023**, *12*, 1128. [CrossRef]
16. Wang, J.; Qiu, S.; Du, J.; Meng, S.; Wang, C.; Teng, F.; Liu, Y. Spatial and Temporal Changes of Urban Built-Up Area in the Yellow River Basin from Nighttime Light Data. *Land* **2022**, *11*, 1067. [CrossRef]
17. Kyba, C.C.M.; Aubé, M.; Bará, S.; Bertolo, A.; Bouroussis, C.A.; Cavazzani, S.; Espey, B.R.; Falchi, F.; Gyuk, G.; Jechow, A.; et al. Multiple Angle Observations Would Benefit Visible Band Remote Sensing Using Night Lights. *J. Geophys. Res. Atmos.* **2022**, *127*, e2021JD036382. [CrossRef]
18. Zheng, Q.; Seto, K.C.; Zhou, Y.; You, S.; Weng, Q. Nighttime light remote sensing for urban applications: Progress, challenges, and prospects. *ISPRS J. Photogramm. Remote Sens.* **2023**, *202*, 125–141. [CrossRef]
19. Zhao, X.; Yu, B.; Liu, Y.; Yao, S.; Lian, T.; Chen, L.; Yang, C.; Chen, Z.; Wu, J. NPP-VIIRS DNB Daily Data in Natural Disaster Assessment: Evidence from Selected Case Studies. *Remote Sens.* **2018**, *10*, 1526. [CrossRef]

20. He, L.; Lv, M.; Zhu, T. Integration of DMSP-OLS and NPP-VIIRS nighttime light remote sensing images. *Bull. Surv. Mapp.* **2023**, *1*, 31–38. [CrossRef]
21. Yuan, Y.; Wang, C.; Liu, S.; Chen, Z.; Ma, X.; Li, W.; Zhang, L.; Yu, B. The Changes in Nighttime Lights Caused by the Turkey–Syria Earthquake Using NOAA-20 VIIRS Day/Night Band Data. *Remote Sens.* **2023**, *15*, 3438. [CrossRef]
22. Yuan, Y.; Chen, Z. The impacts of land cover spatial combination on nighttime light intensity in 2010 and 2020: A case study of Fuzhou, China. *Comput. Urban Sci.* **2023**, *3*, 5. [CrossRef]
23. Zhao, F.; Ding, J.; Zhang, S.; Luan, G.; Song, L.; Peng, Z.; Du, Q.; Xie, Z. Estimating Rural Electric Power Consumption Using NPP-VIIRS Night-Time Light, Toponym and POI Data in Ethnic Minority Areas of China. *Remote Sens.* **2020**, *12*, 2836. [CrossRef]
24. Shi, K.; Chen, Z.; Cui, Y.; Wu, J.; Yu, B. NPP-VIIRS Nighttime Light Data Have Different Correlated Relationships with Fossil Fuel Combustion Carbon Emissions from Different Sectors. *IEEE Geosci. Remote Sens. Lett.* **2020**, *18*, 2062–2066. [CrossRef]
25. Wu, B.; Yang, C.; Wu, Q.; Wang, C.; Wu, J.; Yu, B. A building volume adjusted nighttime light index for characterizing the relationship between urban population and nighttime light intensity. *Comput. Environ. Urban Syst.* **2023**, *99*, 101911. [CrossRef]
26. Yu, B.; Shi, K.; Hu, Y.; Huang, C.; Chen, Z.; Wu, J. Poverty Evaluation Using NPP-VIIRS Nighttime Light Composite Data at the County Level in China. *IEEE J. Sel. Top. Appl. Earth Obs. Remote Sens.* **2015**, *8*, 1217–1229. [CrossRef]
27. Zhang, Z.; Wang, J.; Xiong, N.; Liang, B.; Wang, Z. Air Pollution Exposure Based on Nighttime Light Remote Sensing and Multi-source Geographic Data in Beijing. *Chin. Geogr. Sci.* **2023**, *33*, 320–332. [CrossRef]
28. Xie, Z.; Yuan, M.; Zhang, F.; Chen, M.; Tian, M.; Sun, L.; Su, G.; Liu, R. A Structure Identification Method for Urban Agglomeration Based on Nighttime Light Data and Railway Data. *Remote Sens.* **2023**, *15*, 216. [CrossRef]
29. Fan, X.; Nie, G.; Deng, Y.; An, J.; Zhou, J.; Li, H. Rapid detection of earthquake damage areas using VIIRS nearly constant contrast night-time light data. *Int. J. Remote Sens.* **2019**, *40*, 2386–2409. [CrossRef]
30. Li, X.; Zhan, C.; Tao, J.; Li, L. Long-Term Monitoring of the Impacts of Disaster on Human Activity Using DMSP/OLS Nighttime Light Data: A Case Study of the 2008 Wenchuan, China Earthquake. *Remote Sens.* **2018**, *10*, 588. [CrossRef]
31. Liu, Y.; Liu, W.; Lin, Y.; Zhang, X.; Zhou, J.; Wei, B.; Nie, G.; Gross, L. Urban waterlogging resilience assessment and postdisaster recovery monitoring using NPP-VIIRS nighttime light data: A case study of the 'July 20, 2021' heavy rainstorm in Zhengzhou City, China. *Int. J. Disaster Risk Reduct.* **2023**, *90*, 103649. [CrossRef]
32. Chen, Z.; Yu, S.; You, X.; Yang, C.; Wang, C.; Lin, J.; Wu, W.; Yu, B. New nighttime light landscape metrics for analyzing urban-rural differentiation in economic development at township: A case study of Fujian province, China. *Appl. Geogr.* **2023**, *150*, 102841. [CrossRef]
33. Yang, J.; Li, W.; Chen, J.; Sun, C. Refined Carbon Emission Measurement Based on NPP-VIIRS Nighttime Light Data: A Case Study of the Pearl River Delta Region, China. *Sensors* **2023**, *23*, 191. [CrossRef]
34. Xu, G.; Zeng, T.; Jin, H.; Xu, C.; Zhang, Z. Spatio-Temporal Variations and Influencing Factors of Country-Level Carbon Emissions for Northeast China Based on VIIRS Nighttime Lighting Data. *Int. J. Environ. Res. Public Health* **2023**, *20*, 829. [CrossRef]
35. Wu, S.; Hu, S.; Frazier, A.E.; Hu, Z. China's urban and rural residential carbon emissions: Past and future scenarios. *Resour. Conserv. Recycl.* **2023**, *190*, 106802. [CrossRef]
36. Guo, R.; Leng, H.; Yuan, Q.; Song, S. Impact of Urban Form on CO_2 Emissions under Different Socioeconomic Factors: Evidence from 132 Small and Medium-Sized Cities in China. *Land* **2022**, *11*, 713. [CrossRef]
37. Fang, G.; Gao, Z.; Tian, L.; Fu, M. What drives urban carbon emission efficiency? Spatial analysis based on nighttime light data. *Appl. Energy* **2022**, *312*, 118772. [CrossRef]
38. Doll, C.H.; Muller, J.-P.; Elvidge, C.D. Night-time imagery as a tool for global mapping of socioeconomic parameters and greenhouse gas emissions. *AMBIO J. Hum. Environ.* **2000**, *29*, 157–162. [CrossRef]
39. Sun, Y.; Zheng, S.; Wu, Y.; Schlink, U.; Singh, R.P. Spatiotemporal Variations of City-Level Carbon Emissions in China during 2000–2017 Using Nighttime Light Data. *Remote Sens.* **2020**, *12*, 2916. [CrossRef]
40. Yang, T.; Liu, J.; Mi, H.; Cao, Z.; Wang, Y.; Han, H.; Luan, J.; Wang, Z. An Estimating Method for Carbon Emissions of China Based on Nighttime Lights Remote Sensing Satellite Images. *Sustainability* **2022**, *14*, 2269. [CrossRef]
41. Guo, W.; Li, Y.; Li, P.; Zhao, X.; Zhang, J. Using a combination of nighttime light and MODIS data to estimate spatiotemporal patterns of CO_2 emissions at multiple scales. *Sci. Total Environ.* **2022**, *848*, 157630. [CrossRef] [PubMed]
42. Zhang, Y.; Xu, X. Carbon emission efficiency measurement and influencing factor analysis of nine provinces in the Yellow River basin: Based on SBM-DDF model and Tobit-CCD model. *Environ. Sci. Pollut. Res.* **2022**, *29*, 33263–33280. [CrossRef] [PubMed]
43. Zhang, Y.; Yu, Z. Spatiotemporal evolution characteristics and dynamic efficiency decomposition of carbon emission efficiency in the Yellow River Basin. *PLoS ONE* **2022**, *17*, e0264274. [CrossRef] [PubMed]
44. Zhao, J.; Kou, L.; Wang, H.; He, X.; Xiong, Z.; Liu, C.; Cui, H. Carbon Emission Prediction Model and Analysis in the Yellow River Basin Based on a Machine Learning Method. *Sustainability* **2022**, *14*, 6153. [CrossRef]
45. Shi, K.; Wu, Y.; Liu, S.; Chen, Z.; Huang, C.; Cui, Y. Mapping and evaluating global urban entities (2000–2020): A novel perspective to delineate urban entities based on consistent nighttime light data. *GISci. Remote Sens.* **2023**, *60*, 2161199. [CrossRef]
46. Yin, J.; Yao, M.; Yuan, Z.; Yu, G.; Li, X.; Qi, L. Spatial-temporal variations in vegetation and their responses to climatic and anthropogenic factors in upper reaches of the Yangtze River during 2000 to 2019. *Watershed Ecol. Environ.* **2023**, *5*, 114–124. [CrossRef]
47. Chen, Z.; Yu, B.; Yang, C.; Zhou, Y.; Yao, S.; Qian, X.; Wang, C.; Wu, B.; Wu, J. An extended time series (2000–2018) of global NPP-VIIRS-like nighttime light data from a cross-sensor calibration. *Earth Syst. Sci. Data* **2021**, *13*, 889–906. [CrossRef]

48. Solomon, B.D. Intergovernmental Panel on Climate Change (IPCC). In *Dictionary of Ecological Economics*; Edward Elgar Publishing: Cheltenham, UK, 2023; p. 302.
49. Eggleston, H.S.; Buendia, L.; Miwa, K.; Ngara, T.; Tanabe, K. *2006 IPCC Guidelines for National Greenhouse Gas Inventories*; IPCC: Geneva, Switzerland, 2006.
50. Qiu, S.; Lei, T.; Wu, J.; Bi, S. Energy demand and supply planning of China through 2060. *Energy* **2021**, *234*, 121193. [CrossRef]